Development of the GEOS-5 Atmospheric General Circulation Model: Evolution from MERRA to MERRA2.

Andrea Molod[1], Lawrence Takacs[2], Max Suarez[3], and Julio Bacmeister[4]

[1]University of Maryland College Park, College Park, MD
[2]Science Systems and Applications, Inc., Lanham, MD
[3]NASA Goddard Space Flight Center, Greenbelt, MD
[4]National Center for Atmospheric Research, Boulder, CO
[5]Center for Next Generation Numerical Model, Seoul, Korea

Correspondence to: Andrea Molod
(Andrea.Molod@nasa.gov)

Abstract.

The Modern-Era Retrospective Analysis for Research and Applications-2 (MERRA2) version of the GEOS-5 Atmospheric General Circulation Model (AGCM) is currently in use in the NASA Global Modeling and Assimilation Office (GMAO) at a wide range of resolutions for a variety of applications. Details of the changes in parameterizations subsequent to the version in the original MERRA reanalysis are presented here. Results of a series of atmosphere-only sensitivity studies are shown to demonstrate changes in simulated climate associated with specific changes in physical parameterizations, and the impact of the newly implemented resolution-aware behavior on simulations at different resolutions is demonstrated. The GEOS-5 AGCM presented here is the model used as part of the GMAO's MERRA2 reanalysis, the global mesoscale "nature run", the real-time numerical weather prediction system, and for atmosphere-only, coupled ocean-atmosphere and coupled atmosphere-chemistry simulations.

The seasonal mean climate of the MERRA2 version of the GEOS-5 AGCM represents a substantial improvement over the simulated climate of the MERRA version at all resolutions and for all applications. Fundamental improvements in simulated climate are associated with the increased re-evaporation of frozen precipitation and cloud condensate, resulting in a wetter atmosphere. Improvements in simulated climate are also shown to be attributable to changes in the background gravity wave drag, and to upgrades in the relationship between the ocean surface stress and the ocean roughness. The series of "resolution aware" parameters related to the moist physics were shown to result in improvements at higher resolutions, and result in AGCM simulations that exhibit seamless behavior across different resolutions and applications.

1

1 Introduction

The various activities of NASA's Global Modeling and Assimilation Office (GMAO) neccesitate a model that can function seamlessly across many different resolutions and applications. These applications include real-time atmospheric analyses and forecasts at a resolution of 0.25°, long term reanalyses at 0.5°, coupled atmosphere-ocean and coupled atmosphere-chemistry simulations at 1-2°, and global mesoscale simulations at 7km. The Modern-Era Retrospective Analysis for Research and Applications-2 (MERRA2) version of the GEOS-5 AGCM is part of an ongoing development of a new generation AGCM at GMAO. The focus of the development of the MERRA version of the GEOS-5 AGCM was on the behavior of the components of the hydrological cycle in reanalysis mode, while the focus of the development of the MERRA2 AGCM was on a model that functions seamlessly in numerical weather prediction, reanalysis, climate and global mesoscale modes. To this end, some of the physical parameterizations were replaced, some parameters governing the behavior of other physical parameterizations were changed, and resolution-aware parameters were implemented in the moist process parameterizations.

Many studies exist that describe major improvements in new versions of AGCMs and show the improvements in simulations as compared to reanalyses and other observations (ie., Neale et al., 2013, Donner, et al., 2011, Pope et al., 2000). The present study adds to that type of analysis by carefully documenting the connection between individual changes in the physical parameterizations of the AGCM and improvements in the climate simulation at coarse resolution. A series of sensitivity experiments were conceived and analyzed to explore, step by step, each important change in parameterizations between the MERRA and MERRA2 AGCMs, and to demonstrate the impact on the simulated climate. The present study also describes and analyzes the improvements in high resolution simulations due to some changes in parameterizations specifically targeted for those resolutions.

The details of the changes in the AGCM physical parameterizations are described in the next section, the step by step experiments to isolate the impacts of these changes are described in section 3, and the impacts of the "resolution aware" aspects of the AGCM are described in section 4. The study is summarized in section 5.

2 Description of the MERRA2 version of the GEOS-5 AGCM

The generation of the GEOS-5 Atmospheric General Circulation Model (GCM) that was used as part of NASA's Modern-Era Retrospective Analysis for Research and Applications (MERRA) is described in Rienecker, et al. (2008), and most of the subsequent development of the physical parameterizations for the current, MERRA2 version is described in Molod et al. (2012). In addition to the changes in the physical parameterizations, the development of the MERRA2 AGCM also included two fundamental elements that will not be addressed in the present study. The horizontal

2

discretization of the MERRA2 AGCM is computed on the cubed sphere grid of Putman and Lin (2007), although it still retains the option to use the latitude/longitude discretization. The cubed sphere grid allows for the relative uniformity of grid spacing at all latitudes, and avoids the grid

60   spacing singularities found in the latitude/longitude grid. In addition, the MERRA2 AGCM has been modified to account for the change in total mass due to the change in total water content computed in the moist and turbulence processes. The total mass of each layer is adjusted to include these changes in total water content, and the associated adjustment is then made to the specific masses of all constituents, including water substances. The benefit for the AGCM mean simulated climate

65   is small, but results in the conservation of dry mass during the simulation. The algorithm for this adjustment and the benefits for AGCM simulations and data assimilation experiments are described in detail in Takacs et al. (2014).

    A brief summary of the model's physical parameterizations relevant to the present study is provided here. The GEOS-5 AGCM physics includes parameterization schemes for atmospheric con-

70   vection, large scale precipitation and cloud cover, longwave and shortwave radiation, turbulence, gravity wave drag, a land surface model, a thermodynamic sea ice model, and a simple glacier model.

    Convection is parameterized using the Relaxed Arakawa-Schubert (RAS) scheme of Moorthi and Suarez (1992) and includes a scheme for the generation and re-evaporation of falling rain (Bacmeis-

75   ter et al., 2006). A "stochastic Tokioka trigger" function (Bacmeister and Stephens, 2011) governs the upper limits on the allowable entrainment by sampling from a probability distribution function with specified parameters. The prognostic cloud cover and cloud water and ice scheme is from Bacmeister et al. (2006). The scheme includes large scale condensation governed by the probability distribution function described in Molod (2012), evaporation, autoconversion and accretion of cloud

80   water and ice, sedimentation of cloud ice and re-evaporation of falling precipitation.

    The turbulence parameterization is based on the non-local scheme of Lock (2000) scheme, acting together with the Richardson-number based scheme of Louis and Geleyn (1982). The original Lock scheme was extended in GEOS-5 to include moist heating and entrainment in the unstable surface parcel calculations. The Monin-Obukhov similarity theory based parameterization of surface layer

85   turbulence is described in Helfand and Schubert (1995), and includes the effects of a viscous sublayer for heat and moisture transport over all surfaces except land. The ocean roughness is determined by a polynomial which is a blend of the algorithms of Large and Pond (1981) and Kondo (1975), modified in the mid-range wind regime based on recent observations in the southern ocean according to Garfinkel et al. (2011) and in the high wind regime according to Molod et al. (2013).

90   The longwave radiative processes are described by Chou and Suarez (1994), and the shortwave radiative processes are from Chou and Suarez (1999). The gravity wave parameterization computes the momentum and heat deposition into the grid-scale flow due to orographic (McFarlane, 1987) and nonorographic (after Garcia and Boville, 1994) gravity wave breaking. The Land Surface Model

from Koster et. al (2000) is a catchment-based scheme that treats subgrid scale heterogeneity in
surface moisture statistically. Glacial thermodynamic process are parameterized using an adaptation
of the Stieglitz et al. (2001) snow model to glacial ice (Cullather et al., 2014), and the catchment
and glacier models are each coupled to the multi-layer snow model of Stieglitz et al. (2001). Sea ice
albedos in the northern hemisphere are from the monthly mean observations of Duynkerke and de
Roode (2001).

3   Evolution of Low Resolution Simulated Climate from MERRA AGCM to MERRA2 AGCM

The mean climate characteristics of a single 30-year MERRA2 AGCM simulation on the lati-
tude/longitude grid at a horizontal resolution of 0.5° x 0.5° were evaluated by comparison with
reanalysis and with different satellite and *in situ* based observational estimates (Molod et al., 2012).
They found substantial improvements in some key aspects of the mean circulation in the MERRA2
version of the GEOS-5 AGCM, and also reported on existing discrepancies between the modeled and
observed climates. Here we present the results of a series of experiments designed to attribute each
fundamental improvement in AGCM simulated climate to a specific change in parameterization.

The experiments to be described in this section were all conducted on the latitude/longitude grid
at 2.° x 2.5° horizontal resolution, on a vertical hybrid eta-pressure coordinate grid with 72 levels,
spaced to increase the resolution near the surface and near the tropopause. The simulations were
all forced with observed sea surface temperatures (Reynolds, 2002), and ran for 30 years each.
The sequence of experiments was designed to start with the MERRA2 AGCM as the control and
backtrack, one parameterization change at a time or small groups of parameterization changes as
a time, to a model that replicates the MERRA AGCM simulated climate. The parameterization
changes are listed in table 1, and the full sequence of the control and 7 sensitivity experiments to be
described in this section is listed in Table 2.

3.1   Ocean Surface Winds

The parameterization of the surface layer turbulence in the MERRA2 AGCM includes a substantial
modification of the functional relationship between ocean surface roughness and wind stress, shown
in Figure 1. The relationship for the moderate range surface wind speeds from the MERRA AGCM
(green) and the MERRA2 AGCM (black) is shown in figure 1a, where the increased roughness
based on the implementation of Garfinkel et al. (2011) is apparent. The first experiment in the
series, experiment 1, reverts back to the formulation for the relationship between ocean surface
roughness and stress used in the MERRA AGCM. The effect for simulations at 2.° x 2.5° resolution
is expected be an increase in the experiment 1 simulated surface wind speeds in the mid-range of
wind speeds, that is, in the 5 m s^{-1} to 25 m s^{-1} range. Figure 1b shows the relationship between
wind speed and roughness for a larger range of wind speeds after Molod et al. (2013), where the

4

reduction of roughness at speeds greater than approximately 30 m s^{-1} is apparant. This change is expected to result in a net increase of wind speeds in higher wind regimes as was shown in Molod et al. (2013) for simulations at 0.25 ° resolution, but this impact is not apparent at the resolution of the experiments described here because the simulated wind speeds generally do not reach 30 m s^{-1}.

Surface wind speeds from the MERRA2 AGCM control and experiment 1 are shown in figure 2. The change in the simulated surface winds is most apparent in the southern hemisphere, where the Goddard Satellite-based Surface Turbulent Fluxes (GSSTF, Shie et al., 2009) surface winds, seen in figure 2b, show values near 8 m s^{-1}, experiment 1 (2d) shows surface winds near 12 m s^{-1} and the MERRA2 AGCM control (2a) shows surface winds near 10 m s^{-1}. The difference from the GSSTF estimate (shown in 2c and 2f) shows a reduction in the difference from up to 4 m s^{-1} in experiment 1 to a difference of up to 2 m s^{-1} in the MERRA2 AGCM control, pointing out the improvement in AGCM simulated climate due to the change in roughess formulation.

3.2   Quasi-biennial Oscillation

The latitudinal profile of background nonorographic drag in the MERRA2 AGCM was modified to include a specified source related to tropical precipitation in addition to the local maxima related to storm track precipitation. The background profiles used in the MERRA2 and the MERRA AGCMs are shown in figure 3. Experiment 2 of the series examines the impact of the change in the gravity wave drag parameterization of background drag in the tropics, and returns to the MERRA AGCM background drag. Experiment 2 is therefore expected to exhibit a stratospheric wind with no quasi-biennial oscillation (QBO) variability. The tropical (latitude range 10S to 10N) zonal average of the zonal wind as a function of height and time is shown in figure 4. The patterns of large easterly and westerly winds that slant downwards in pressure as time proceeds indicate the downward propagation of the variations due to the QBO. The QBO pattern is seen in figure 4a and 4c, which are the results from experiment 1 from and MERRA reanalysis (Rienecker, et al., 2011), respectively. Figure 4b, however, that shows the results of experiment 2 that uses the old background drag formulation (from figure 3), shows no QBO pattern of variability.

3.3   Stable Surface Layer Fluxes

The parameterization of the surface layer in the MERRA2 AGCM uses the scheme of Helfand and Schubert (1995) based on Monin-Obhukov (MO) similarity theory. The scheme replaced the Louis (1979) scheme used in the MERRA AGCM. The implementation of the MO scheme included the use of a different set of stable layer stability functions, and a different formulation for the viscous sublayer (the laminar layer that can act to impede the flux of heat and moisture). The stable surface layer stability functions in the Helfand scheme result in an increased turbulent heat exchange (of both signs) under stable conditions. Figure 5 shows a scatter diagram of the sensible heat flux as a function of surface bulk Richardson number under conditions where the monthly mean air

temperature exceeds the monthly mean skin temperature. The black points are from the simulation with the Helfand surface layer, and the red are from the simulation using the Louis scheme. The larger values of sensible heat flux in the Helfand simulation are apparent, and even more apparent when the monthly mean sensible heat flux is downward.

Experiment 3 was designed to examine the impact of the change in the surface layer parameterization by reverting back from the Helfand and Schubert scheme to the Louis scheme. Figure 6 shows the sensible heat flux from experiments 2 and 3 along with the difference between them. The differences shown here are attributable to the removal of the viscous sublayer over land in the Helfand and Schubert scheme and to the change in the stable layer stability functions. Figure 6c shows that over most land surfaces the difference in sensible heat flux is negative, indicating less sensible heating when using the Louis scheme. This sign of the difference is consistent with the removal of the viscous sublayer over land surfaces in the Helfand scheme, that would remove some resistance to turbulent exchange that is present over unvegetated land surfaces in the Louis scheme due to the viscous sublayer. Figure 6c also shows regions where the sensible heat flux is greater in the Louis scheme than in the Helfand scheme. These are regions where the surface layer is stable, and where the sensible heat itself is largely downward (that is, the air temperature is greater than the skin temperature). The change in stability functions between the Louis and Helfand scheme, that allows more turbulent exchange in the Helfand scheme, is consistent with the sign of the difference in sensible heat flux in regions where the heat flux is downward.

3.4 Atmospheric Moisture, Clouds and Stationary Wave Pattern

3.4.1 Critical Relative Humidity

The algorithm for large scale condensation, as described in Bacmeister et al. (2006), assumes that the probability distribution function (PDF) of total water is "top-hat" shaped. The width of the PDF can be shown to be associated with a "critical relative humidity" (RH_{crit}) that governs cloud macrophysical and microphysical processes such as condensation and evaporation (Molod, 2012). The relationship between RH_{crit} and PDF width is such that a wider PDF corresponds to a lower RH_{crit}. The MERRA2 AGCM RH_{crit} (Molod, 2012) represents a change in both the magnitude and vertical structure from the RH_{crit} in the MERRA AGCM. Typical RH_{crit} profiles from the MERRA and MERRA2 AGCMs are shown in figure 7, and indicate generally lower values in the MERRA2 AGCM formulation except in the boundary layer, where turbulent mixing is sufficient to homogenize the total water distribution and so result in narrower PDF.

Experiment 5 was designed to examine the impact of the change in RH_{crit}. Removing this change, which for much of the atmosphere means a larger RH_{crit}, should result in a simulation that is generally wetter because the atmosphere is being adjusted back to a higher relative humidity (RH). The zonal mean relative humidity from experiments 4 and 5, along with the difference between

them, is shown in figure 8. The experiment 5 minus experiment 4 difference shows a clear increase in relative humidity in the MERRA AGCM-like experiment due to the increase in RH_{crit}. Relative to available observational verification, the MERRA2 AGCM shows a general wet bias (Molod et al., 2012), which means that the experiment 4 relative humidity field is closer to the observed than experiment 5's RH field.

In addition to having a substantial impact on atmospheric moisture, the change in RH_{crit} also had an impact on the distribution of cloud cover. The higher RH_crit simulation (the MERRA AGCM-like experiment) could either be expected to have less cloud cover because the atmosphere must contain more moisture before new cloud water will be condensed, or could be expected to have more cloud cover due to the feedback of a generally moister atmosphere. Figure 9 shows the zonal mean cloud cover from experiments 4 and 5, and an observational estimate of zonal mean cloud cover from AIRS. The MERRA AGCM-like experiment, experiment 5 (figure 9a), shows increased cloud cover in the 300-600 mb range relative to the MERRA2 AGCM-like experiment, in particular at high latitudes in both hemispheres. In this regard, the MERRA2 AGCM-like experiment result more closely resembles the AIRS cloud cover estimate (figure 9c). This result confirms the hypothesis that higher RH_{crit} results in an atmosphere that is wetter in the mean and has more cloud. The MERRA-like AGCM result (experiment 5) also shows smaller cloud cover near the boundary layer at almost all latitudes. At high latitudes, the MERRA2 AGCM-like boundary layer cloud more closely resembles the AIRS estimate, in the tropics the MERRA2 AGCM-like boundary layer cloud is larger than AIRS, while the MERRA AGCM-like boundary layer cloud is smaller. The change in boundary layer cloud between the MERRA AGCM-like experiment and the MERRA2 AGCM-like experiment is not consistent with the free atmosphere response to the RH_{crit} change because the presence of boundary layer turbulence makes RH_{crit} less of a determining factor for model mean relative humidity there.

3.4.2   Re-evaporation of Precipitation and Condensate

The MERRA2 AGCM scheme for the re-evaporation of precipitation and suspended cloud water and ice contains a series of new parameter settings that result in a substantial increase over the MERRA model in the re-evaporation of snow and ice. The impact of the changes in parameter settings on the water vapor source due to re-evaporation for the December-January-February average is shown in figure 10. The largest increase in the MERRA2 AGCM is aloft, near 500 mb, where the increase is up to 0.7 g kg^{-1} day^{-1}.

Experiment 6 examines the impact of the change in re-evaporation of snow and ice in the MERRA2 AGCM, that is perhaps the most crucial parameterization change. The removal of this change is expected to result in a drier atmosphere, in particular aloft. Because of the importance of this change in parameterization, this simulation is expected to resemble in large part the climatology of the AGCM used as part of MERRA. Figure 11 shows the direct impact of the change from the MERRA2 AGCM

7

to the MERRA AGCM re-evaporation, and, as expected, shows the drying related to the reduced re-evaporation in the MERRA AGCM-like experiment. Figures 11a-c show the change in total precipitable water, and the difference (MERRA AGCM formulation minus MERRA2 AGCM formulation, shown in 11c) is always negative everywhere. The vertical distribution of the moisture is shown with the specific humidity in figures 11d-f, where the difference plot (11f) also shows an almost global reduction in atmospheric water vapor.

The resulting mean circulation in boreal winter underwent a substantial change associated with this drying, and represents the most substantial impact on the simulated climate of all the elements of the MERRA AGCM to MERRA2 AGCM transition. Figure 12 shows the subtantial impact that changing the moisture levels had on the 30-year averaged December-January-February total precipitation. Given the Global Precipitation Climatology Project (GPCP, Huffman et al., 1995) climatology as a reference, the MERRA2 AGCM-like experiment (experiment 5, figure 12d) exhibits an Intertropical Convergence Zone (ITCZ) structure that is properly placed in longitude, a South Pacific Convergence Zone (SPCZ) that properly slants from the western Pacific to the southeast, and more accurately simulated storm track maxima. The precipitation field represents improvements in all these areas related to the MERRA AGCM-like simulation (experiment 6) shown in figure 12a. The change in the tropical precipitation field related to the additional drying in experiment 6 also resulted in substantial changes in the Pacific teleconnection patterns, specifically the Pacific-North-America (PNA) pattern in boreal winter. The eddy height field is an indicator of the strength of the PNA, and is shown in figure 13 in relation to the eddy height from MERRA reanalysis. The MERRA2 AGCM-like simulated PNA pattern (figure 12d) has a stronger and more properly oriented ridge near the west coast of North America relative to the PNA as simulated by the MERRA AGCM-like experiment (figure 12a). This change has implications for the poleward propagation of heat and momentum. The standard deviation of the difference from MERRA reanalysis estimates is also substantially reduced in experiment 5 (16.8 m) relative to experiment 6 (20.3 m). The direct impact of the change in re-evaporation was also evident in the boreal summer climatology. Figure 14 shows this both in the total precipitable water fields and in the specific humidity fields, that exhibit differences between experiments 5 and 6 that are of the order of the differences seen in boreal winter. The impact on the mean summertime circulation, however, was minimal.

3.5 Breakup of the Southern Hemisphere Stratospheric Jet

The changes to the gravity wave drag parameterization included the modification of the "intermittency factor", used to reduce the strength of the gravity wave drag based on expected departure from linear theory. The value of the intermittency factor was increased in the MERRA2 AGCM for orographic waves as a function of latitude, changing from a MERRA AGCM global value of 0.125 to values reaching 0.3125 south of approximately 40°S.

Experiment 7 is the last experiment in the series, incorporating the effects of all the fundamental

270 changes between the MERRA and MERRA2 versions of the GEOS-5 AGCM. The removal of the intermittency change is expected to decrease the orographically induced drag in the southern hemisphere, thereby depositing less momentum aloft and increasing the strength of the westerlies. The zero-wind contour in the southern hemisphere can be used as an indicator of the level and timing of the stratospheric jet breakup. Figure 15 shows the zero-wind contour from experiment 7, experiment

275 6, and MERRA. At the 2 degree horizontal resolution of the simulations described here, the zero wind line is higher in altitude and delayed in time relative to MERRA in both simulations, reflecting a delayed stratospheric jet breakup. The decreased intermittency factor in experiment 7, however, delays the jet breakup even more, showing the improvement in the MERRA2 AGCM-like simulation relative to the MERRA AGCM-like simulation. At higher spatial resolution (not shown) the increase

280 of intermittency factor in the MERRA2 AGCM is effective in producing a reasonable evolution of the polar vortex breakdown in the southern Hemisphere.

4   High resolution simulations and resolution aware behavior in the MERRA2 AGCM

The modifications to the MERRA2 AGCM physical parameterizations described above resulted in improvements in simulated climate at all the resolutions relevant to GMAO. Additional develop-

285 ments were implemented in the MERRA2 AGCM that were particularly applicable to higher resolution (0.25° or higher) simulations. These included the changes in ocean surface roughness at high wind speeds (mentioned in section 3.1 and examined in detail in Molod et al., 2013) and the implementation of "resolution aware" parameters.

The implementation of the "resolution aware" behavior of the moist processes in the MERRA2

290 version of the GEOS-5 AGCM was designed to improve the behavior of the high resolution simulations and to ensure more uniformity of model mean state across resolutions and applications. Figure 16 shows an example of the undesireable behavior in the MERRA version of the AGCM that the "resolution aware" parameters were meant to address. Panels 16a-c show the specific humidity at 1.°, 0.5° and 0.25° resolution, and panels 16g-i show the increase of the bias in atmospheric mois-

295 ture content relative to EC-Interim reanalysis (Dee et al., 2011) as the resolution increases. In order to mitigate this change in simulated climate with increasing resolution, the MERRA2 AGCM moist physics was modified to include two governing parameters that are specified *a priori* as a function of horizontal resolution. These are the critical relative humidity used for large scale condensation, and a parameter which governs the minimum allowable entrainment used for the "stochastic Tokioka

300 trigger" of the convective parameterization.

The dependance of RH_{crit} on horizontal resolution is based on the Molod (2012) analysis of a global mesoscale simulation, and is such that the RH_{crit} increases with finer resolution, as was seen in the progression from the 2° resolution curve up to the 0.25° curve in figure 7. This progression is consistent with an intuitive expectation that the variability of total water within an AGCM grid

9

305 cell decreases as the grid cell becomes smaller. The implementation of the horizontal resolution dependance of RH_{crit} (as described in section 2) in the MERRA2 AGCM resulted in an atmospheric moisture field that is more consistent across different resolutions, as seen in figure 17.

The MERRA2 version of the GEOS-5 AGCM also includes a horizontal resolution dependant and stochastic Tokioka (1988) type trigger (described in Bacmeister and Stephens, 2011) as part of
310 the RAS convective parameterization. The cloud model in RAS computes the effect of individual entraining cloud plumes, and the trigger acts to effectively eliminate any cloud plume with too small an entrainment during ascent. Bacmeister and Stephens (2011) examined the observed relationship between the neutral bouyancy level of a particular sounding and the observed condensate (a proxy for the convective detrainment level), and found that this observational relationship can be approximated
315 by sampling the minimum entrainment from a power law PDF. The parameters of the PDF are specified *a priori*, and vary with resolution. The stochasticity is designed to only occasionally permit the least entraining and therefore the deepest detraining cloud plumes. Lim et al., (2014) reported on a series of sensitivity studies to examine the impact of different choices of the PDF governing parameter on the simulation of strong tropical storms in the GEOS-5 AGCM.

320 The resolution dependance of the stochastic Tokioka trigger is such that it more severely limits the parameterized convective mass flux at high spatial resolution, where we expect the larger scale convective updrafts to be resolved explicitly, and has little impact at low resolution. The change with resolution of the PDF parameters is shown in figure 18, presently specified in an *ad hoc* manner. Figure 19 shows a sequence of the resulting June averaged convective mass fluxes from simulations
325 with different horizontal resolutions. The decrease of parameterized mass flux with resolution reflects the increasingly restrictive trigger, selected from the PDFs with increasingly higher mimimum entrainment values shown in figure 18. The effect of this repressed RAS mass flux on the simulated climate is reflected in the total change in moisture due to moist processes, shown in figure 20. The cloud model in RAS includes a grid scale subsidence to compensate for the updraft mass flux that
330 results in a drying of the sub-cloud layer. Figure 20 shows the decrease of the low level drying with increased horizontal resolution. The benefits of the reduced low level drying and the related maintenance of the cumulus available potential energy during tropical storm development at high resolution was demonstrated in the study of Lim et al. (2014).

5 Conclusions

335 Synthesis and Discussion

The version of the GEOS-5 AGCM used in the Goddard Modeling and Assimilation Office (GMAO) MERRA2 reanalysis was developed for use across many different resolutions and applications. A unique series of AGCM simulations were performed with the GEOS-5 AGCM to detail the impact of each change in parameterization between the MERRA version and the current MERRA2

340 version. The series of sensitivity experiments began with the current AGCM version and regressed, one step of development at a time, to the MERRA AGCM.

The most substantial positive impact on the simulated AGCM climate was shown to be attributable to the increase of the re-evaporation of frozen cloud water and precipitation in the MERRA2 AGCM. The resulting atmosphere had a higher moisture content, and many aspects of the boreal winter

345 climate were substantially improved relative to reanalysis. The moisture and cloud cover amounts were shown to be further improved by the implementation of an AIRS-based PDF of total water.

The development of the MERRA2 AGCM also included the implementation of a set of parameters governing moist processes that contain an *a priori* change in behavior with horizontal resolution. The parameters are ones which govern the mimimum allowable entrainment into a convective up-

350 draft, and govern the atmospheric relative humidity needed for the onset of condensation. Results of a limited set of experiments were shown to demonstrate the benefits of this "resolution aware" behavior at higher resolution.

This study was focused on the results of atmosphere only simulations, but the resulting model has also performed well in coupled atmosphere ocean, coupled atmosphere chemistry, data assimilation,

355 numerical weather prediction and global mesoscale applications.

6   Code Availability

The GEOS-5 source code is available under the NASA Open Source Agreement at http://opensource.gsfc.nasa.gov/projects/GEOS-5/.

11

380 **References**

Bacmeister, J. T., Stephens, G.: Spatial statistics of likely convective clouds in CloudSat data. J. Geophys. Res., 116, D04104, doi:10.1029/2010JD014444, 2011.

Bacmeister, J. T., Suarez, M. J. and Robertson, F. R. : Rain reevaporation, boundary layer–convection interactions, and Pacific rainfall patterns in a AGCM. J.Atmos. Sci., 63, 3383–3403, 2006.

385 Chou, M. -D., and Suarez, M. J.: An efficient thermal infrared radiation parameterization for use in general circulation models. NASA Tech. Memorandum 104606-Vol 3, NASA, Goddard Space Flight Center, Greenbelt, MD, 1994.

Chou, M. -D., and Suarez, M. J.: A Solar Radiation Parameterization for Atmospheric Studies. NASA Tech. Memorandum 104606-Vol 15, NASA, Goddard Space Flight Center, Greenbelt, MD, 1999.

390 Cullather, R. L., Nowicki, S. M. J., Zhao B., and Suarez, M.J.: Evaluation of the surface representation of the Greenland ice sheet in a general circulation model. J. Climate, 27, 4835-4856. doi: 10.1175/JCLI-D-13-00635.1, 2014.

Dee, DP, and co-authors: The ERA-Interim reanalysis: configuration and performance of the data assimilation system. Q. J. R. Meteorol. Soc. 137, 553–597, 2011.

395 Donner, L., and co-authors: The Dynamical Core, Physical Parameterizations, and Basic Simulation Characteristics of the Atmospheric Component AM3 of the GFDL Global Coupled Model CM3 J. Climate, 24, 3484. doi:10.1175/2011JCLI3955.1, 2011.

Duynkerke, P., and de Roode, S.: Surface energy balance and turbulence characteristics observed at the SHEBA Ice Camp during FIRE III. J. Geophys. Res., 106, 15313–15322, doi:10.1029/2000JD900537, 2001.

400 Helfand, H. M., and Schubert, S. D.: Climatology of the Simulated Great Plains Low-Level Jet and Its contribution to the Continental Moisture Budget of the United States. J. Climate, 8, 784-806, 1995.

Huffman, G., Adler, R.F., Rudolf, B., Schneider, U. and Keehn, P.R.: Global precipitation estimates based on a technique for combining satellite-based estimates, rain gauge analysis, and NWP model precipitation information. J. Climate, 8, 1284-1295, 1995.

405 Garcia, R. R., and Boville, B. A.: Downward control of the mean meridional circulation and temperature distribution of the polar winter stratosphere. J. Atmos. Sci., 51, 2238–2245, 1994.

Garfinkel, C.I., Molod, A., Oman, L. D. and Song, I.-S.: Improvement of the GEOS-5 AGCM upon Updating the Air-Sea Roughness Parameterization. Geophys. Res. Lett., 38, L18702, doi:10.1029/2011GL048802, 2011.

410 Kondo, J.: Air-sea bulk transfer coefficients in diabatic conditions. Boundary Layer Meteor., 9, 91-112, 1975.

Koster, R. D., Suarez, M.J., Ducharne, A., Stieglitz, M. and Kumar, P.: A catchment-based approach to modeling land surface processes in a GCM, Part 1, Model structure. J. Geophys. Res., 105, 24 809–24 822, 2000.

Large, W. G., and Pond, S.: Open ocean momentum flux measurements in moderate to strong winds. J. Phys.
415 Oceanogr., 11, 324-336, 1981.

Lim, Y.-K., Schubert, S. D., Reale, O., Lee, M.-I., Molod, A. and Suarez, M. J.: Sensitivity of Tropical Cyclones to Parameterized 2 Convection in the NASA GEOS5 Model. J. Climate, Sub Judice, 2014.

Lock, A. P., Brown, A. R., Bush, M. R., Martin, G. M. and Smith, R. N. B.: A new boundary layer mixing scheme. Part I: Scheme description and single-column model tests. Mon. Wea. Rev., 138, 3187–3199, 2000.

13

420   Louis, J. E.: A Parametric Model of Vertical Eddy Fluxes in the Atmosphere, Bound. Lay. Meteorol., 17, 187-202, 1979.

Louis, J. and Geleyn, J.: A short history of the PBL parameterization at ECMWF. Proc. ECMWF Workshop on Planetary Boundary Layer Parameterization, Reading, United Kingdom, ECMWF, 59–80, 1982.

McFarlane, N. A.: The effect of orographically excited gravity-wave drag on the circulation of the lower strato-
425   sphere and troposphere. J. Atmos. Sci., 44, 1775-1800, 1987.

Molod, A., Suarez, M. J. and Partyka, G.: The impact of limiting ocean roughness on GEOS-5 AGCM tropical cyclone forecasts. Geophys. Res. Lett., 40, 411-415. DOI: 10.1029/2012GL053979, 2013.

Molod, A.: Constraints on the Profiles of Total Water PDF in AGCMs from AIRS and a High-Resolution Model. J. Climate, 25, 8341–8352, 2012.

430   Molod, A., Takacs, L. L., Suarez, M. J., Bacmeister, J. T., Song, I.-S. and Eichmann, A.: The GEOS-5 Atmo-
spheric General Circulation Model: Mean Climate and Development from MERRA to Fortuna. NASA Tech. Memo. 104606, Volume 28, Tech. Rep. Series on Global Modeling and Data Assimilation, Max J. Suarez, ed, 117 pp., 2012.

Moorthi, S., and Suarez, M.J.: Relaxed Arakawa Schubert: A parameterization of moist convection for general
435   circulation models. Mon. Wea. Rev., 120, 978-1002, 1992.

Neale, R. B., Richter, J., Park, S., Lauritzen, P. H., Vavrus, S. J., Rasch, P. J. and Zhang, M.: The Mean Climate of the Community Atmosphere Model (CAM4) in Forced SST and Fully Coupled Experiments, Journal of Climate, 26, p. 5150-5168, doi: 10.1175/JCLI-D-12-00236.1, 2013.

Pope, V. D., Gallani, M. L., Rowntree, P. R. and Stratton, R. A.: The impact of new physical parametrizations in
440   the Hadley Centre climate model - HadAM3. Climate Dynamics, 16, 123-146, doi:10.1007/s003820050009 , 2000.

Rienecker, M. M., and co-authors: The GEOS-5 Data Assimilation System—Documentation of versions 5.0.1 and 5.1.0, and 5.2.0. NASA Tech. Rep. Series on Global Modeling and Data Assimilation, NASA/TM-2008-104606, Vol. 27, 92 pp., 2008.

445   Rienecker, M.M., and co-authors: MERRA: NASA's Modern-Era Retrospective Analysis for Research and Applications. J. Climate, 24, 3624-3648, 2011.

Reynolds, R. W., N. A. Rayner, T. M. Smith, D. C. Stokes, and W. Wang, 2002: An improved in situ and satellite SST analysis for climate. J. Climate, 15, 1609–1625.

Schmidt, G.A. and co-authors:Present day atmospheric simulations using GISS ModelE: Comparison to in-situ,
450   satellite and reanalysis data. J. Climate 19, 153-192, 2006.

Shie, C.-L., Chiu, L. S., Adler, R., Nelkin, E., Lin, I.-I., Xie, P., Wang, F.-C., Chokngamwong, R., Olson, W., and Chu, D. A.: A Note on reviving the Goddard satellite-based surface turbulent fluxes (GSSTF) dataset. Adv. Atmos. Sci., 26(6), 1071-1080, 2009.

Stieglitz, M., Ducharne, A., Koster, R. D. and Suarez, M.J.: The Impact of Detailed Snow Physics on the
455   Simulation of Snowcover and Subsurface Thermodynamics at Continental Scales. J. Hydromet., 2, 228-242, 2001.

Takacs, L., Suarez, M. J. and Todling, R.: Maintaining Atmospheric Mass Balance within Reanalysis. NASA Tech. Memo. 104606, Volume 34 Technical Report Series on Global Modeling and Data Assimilation, R. Koster, ed., 2014.
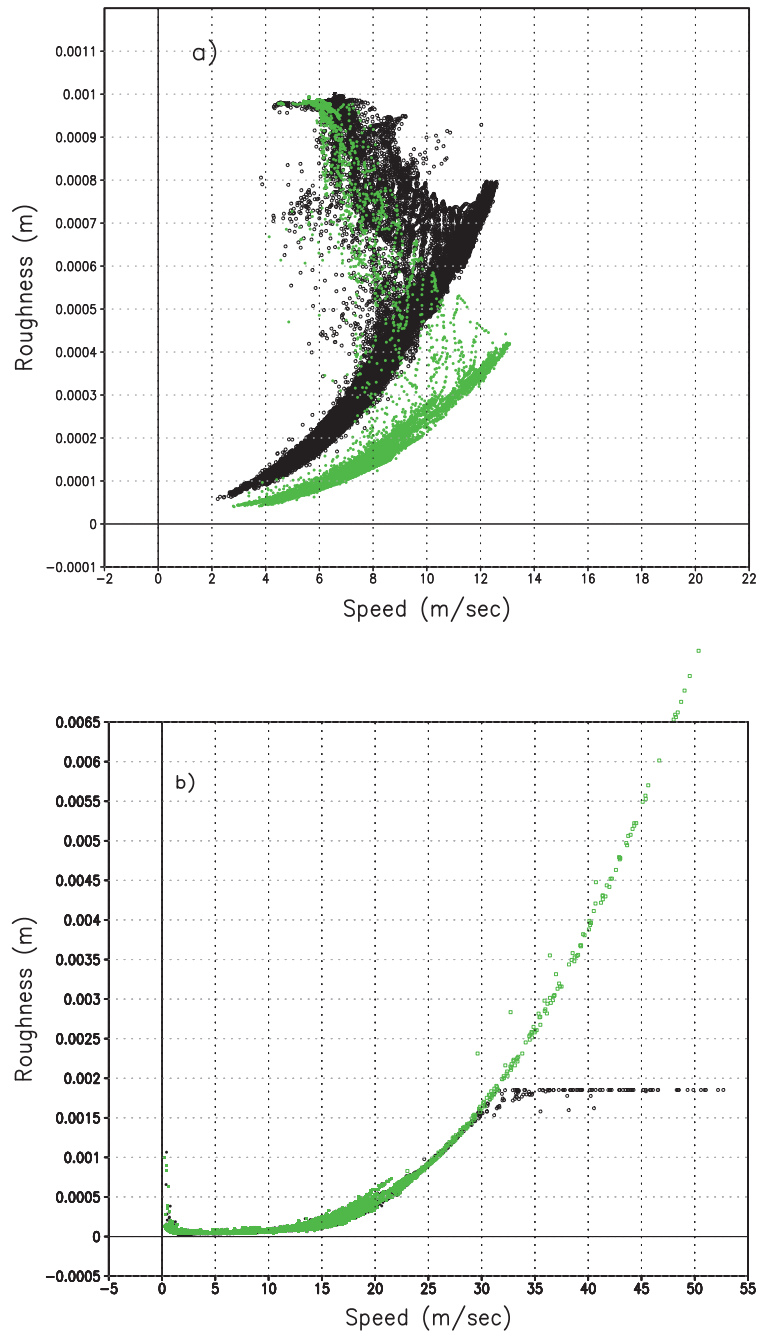
Fig. 1. Scatter diagram of surface wind speed $(\mathrm{m\,sec^{-1}})$ versus ocean roughness (m) in the MERRA and MERRA2 AGCMs. a) diagram focusing on medium range of wind speeds, MERRA2 shown in black and MERRA in green, and b) diagram extending to high wind regimes, MERRA shown in green and MERRA2 in black.
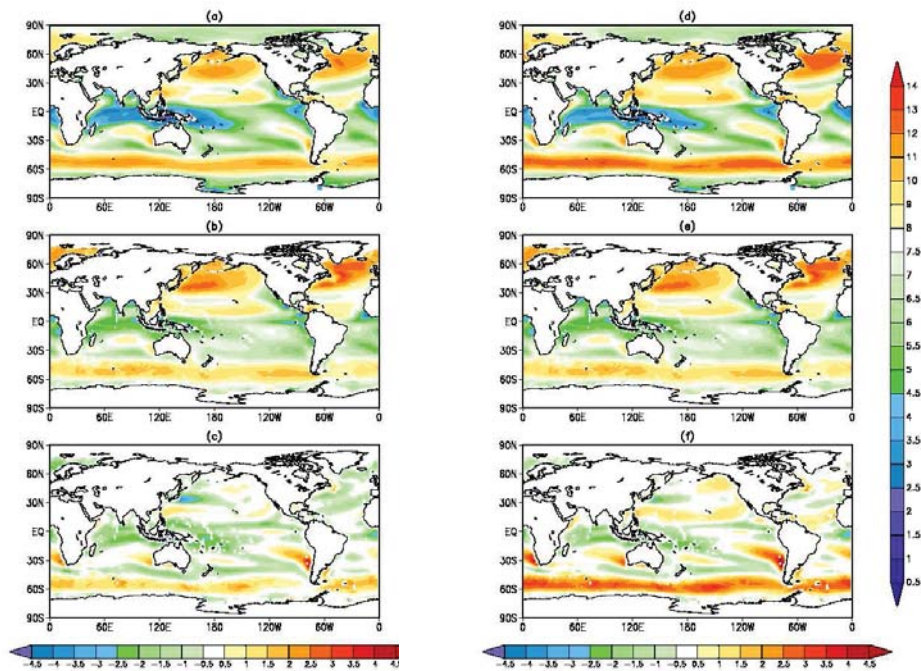
15

Fig. 2. 30-year average December-January-February surface wind speed ($m\,sec^{-1}$) from: a) MERRA2 control, b) GSSTF, c) Control-GSSTF, d) Experiment 1, e) GSSTF, f) Experiment 1-GSSTF

16
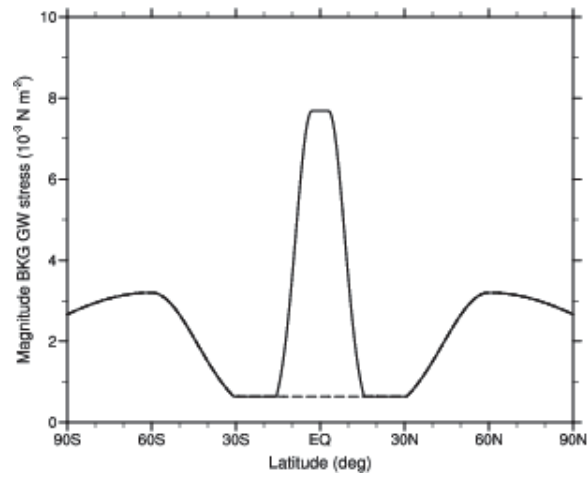
Fig. 3. Background nonorographic drag from the MERRA and MERRA2 AGCM simulations

17
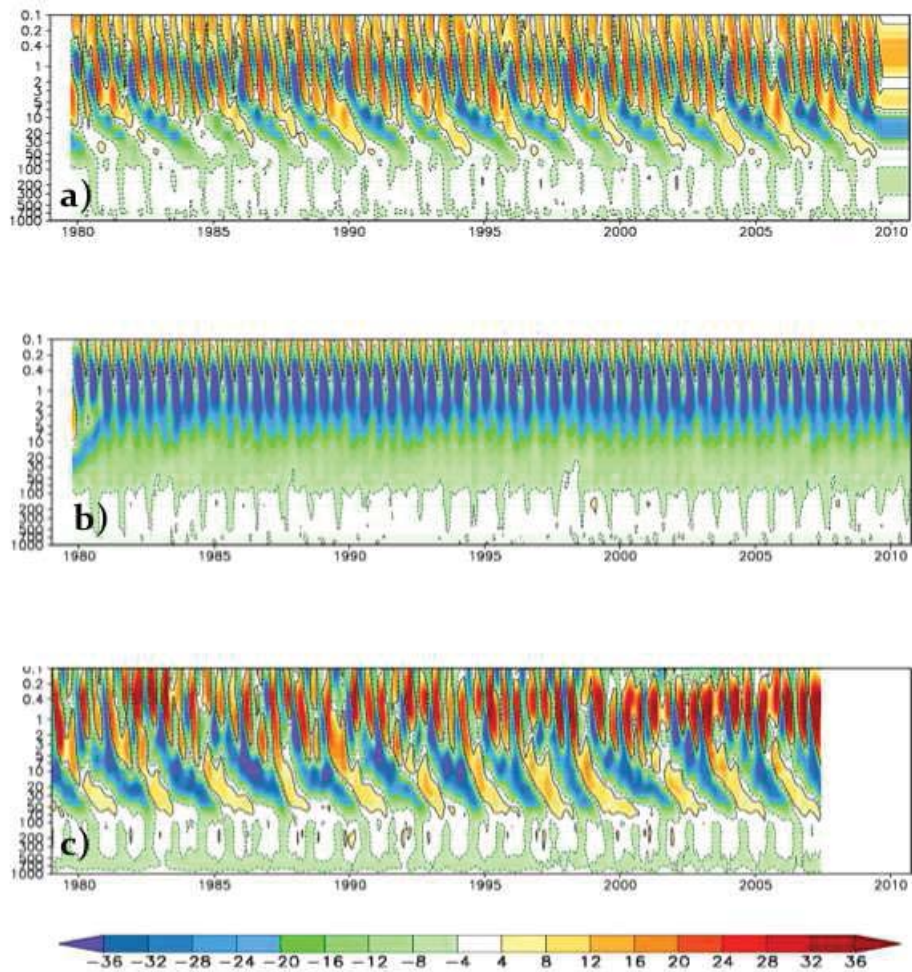
Fig. 4. Spatial average of zonal wind in $\mathrm{m\,s^{-1}}$ from 10S to 10N latitude as a function of pressure level in mb and time from a) MERRA2 control, b) Experiment 2 and c) MERRA reanalysis.
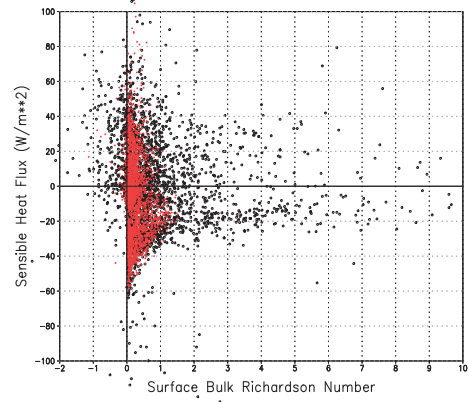
Fig. 5. Surface bulk Richardson number as a function of sensible heat flux in W m^{-2} in a single July from experiment 3 (red) and experiment 2 (black).
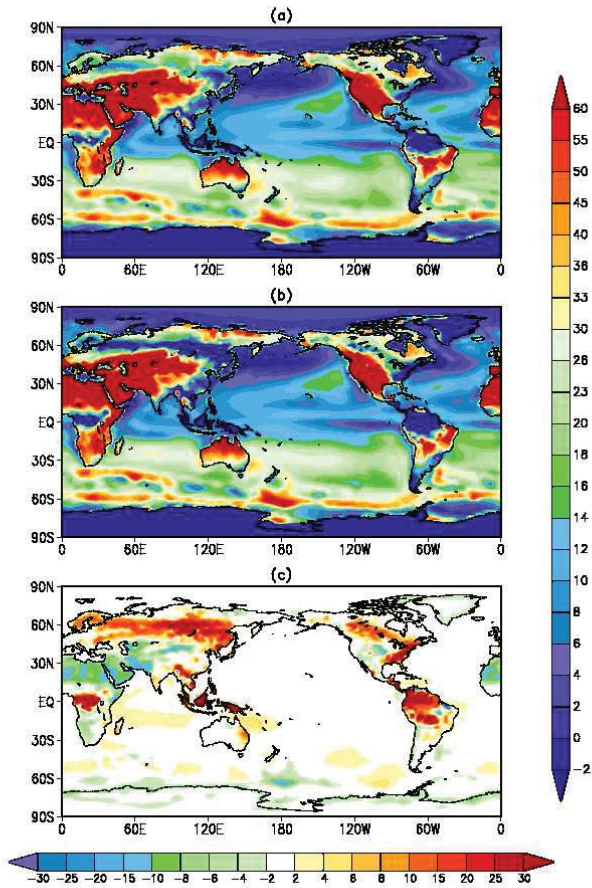
Fig. 6. June-July-August averaged sensible heat flux in $\mathrm{W\,m^{-2}}$ from a) Experiment 3 (Louis scheme), b) experiment 2 (Helfand scheme) and c) the difference, experiment 3 minus experiment 2.
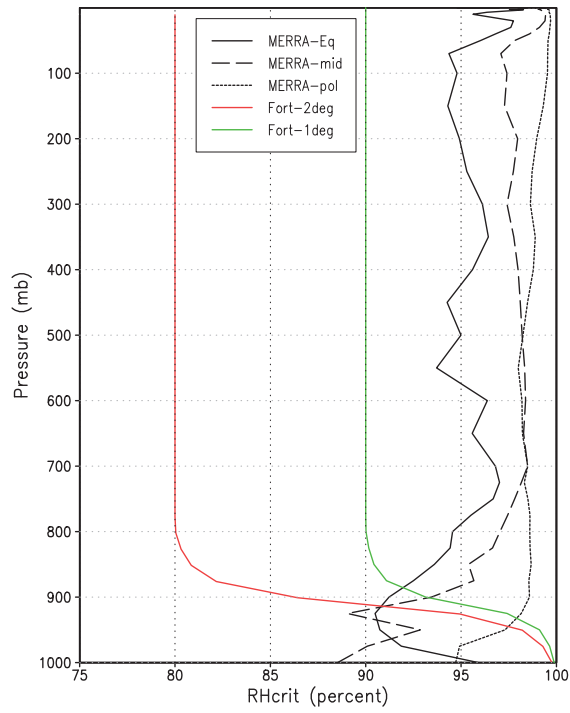
Fig. 7. Critical relative humidity. Black from MERRA AGCM formulation, green from MERRA2 AGCM formulation for 1° resolution, and red from MERRA2 AGCM formulation for 2° resolution.
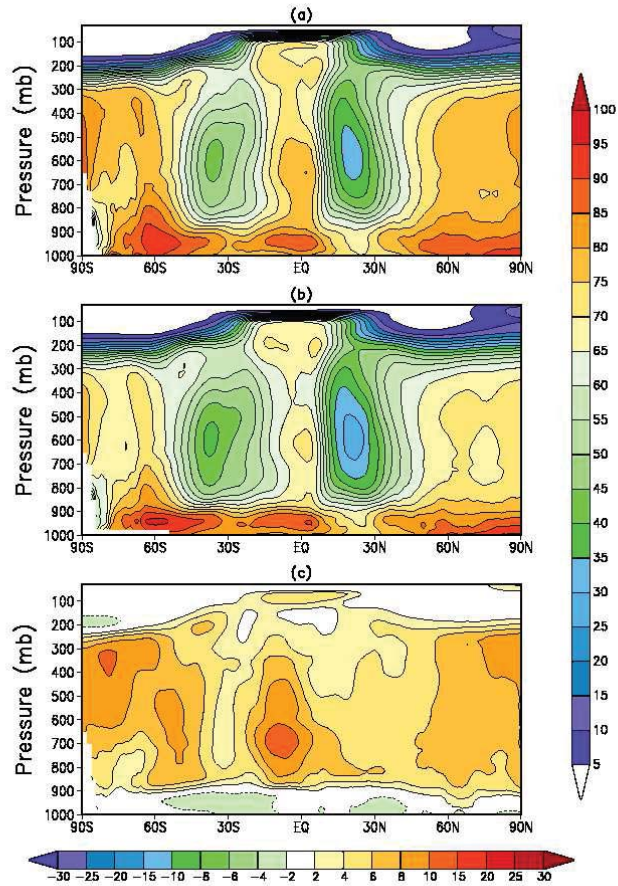
Fig. 8. December-January-February averaged relative humidity in percent from a) Experiment 5 (MERRA AGCM-like), b) experiment 4 (MERRA2 AGCM-like) and c) the difference, experiment 5 minus experiment 4.

22
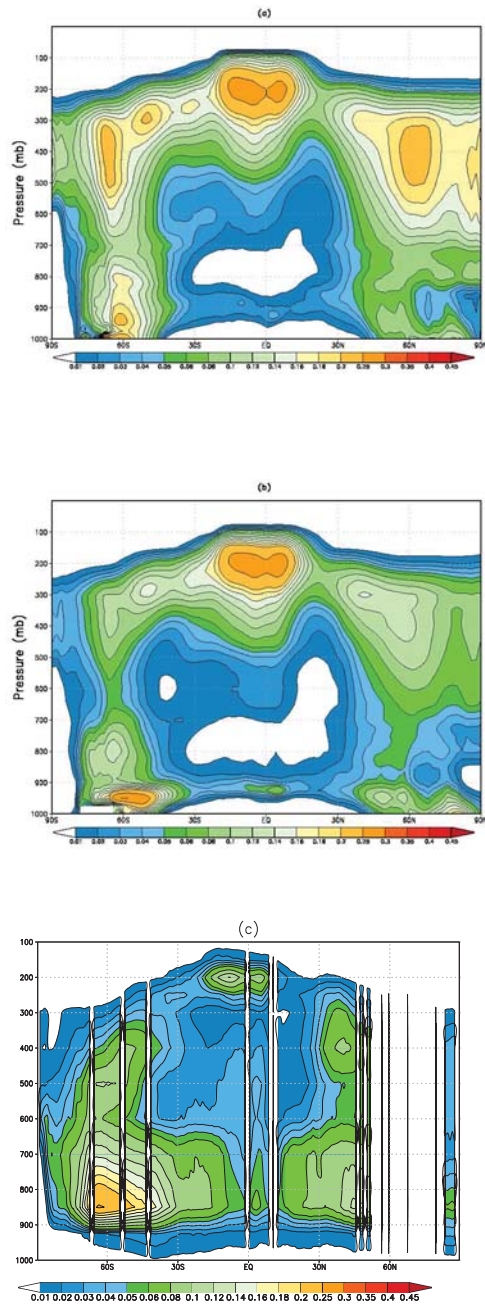
Fig. 9. December-January-February averaged cloud fraction from a) Experiment 5 (MERRA AGCM-like), b) experiment 4 (MERRA2 AGCM-like) and c) AIRS retreivals

23
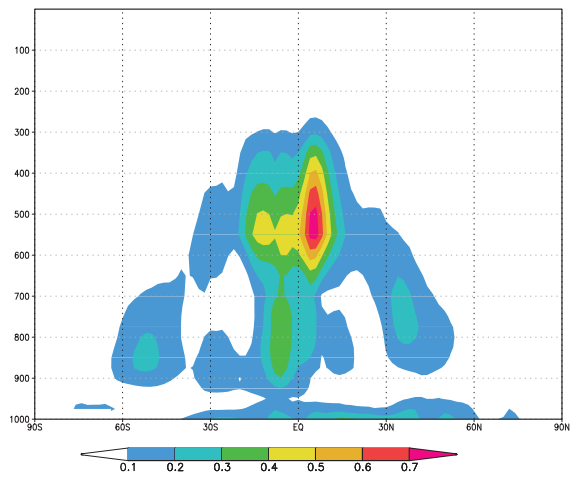
Fig. 10. The difference (MERRA2 AGCM-like minus MERRA AGCM-like) of zonal mean specific humidity source term due to all re-evaporation for December-January-February.
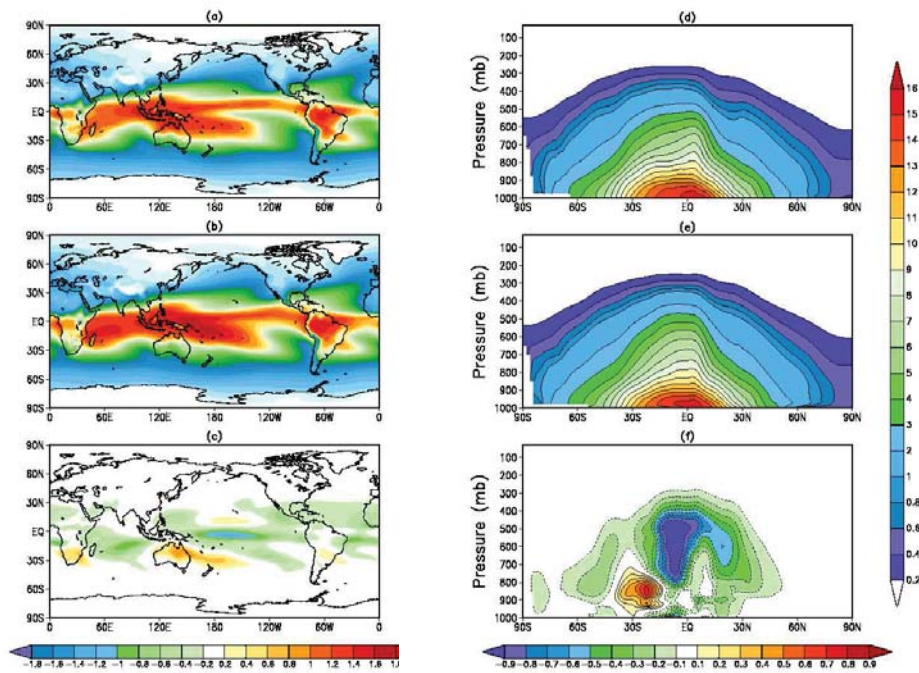
Fig. 11. a) December-January-February total precipitable water in mm from experiment 6 (MERRA AGCM-like), b) same as a) but from experiment 5, c) sa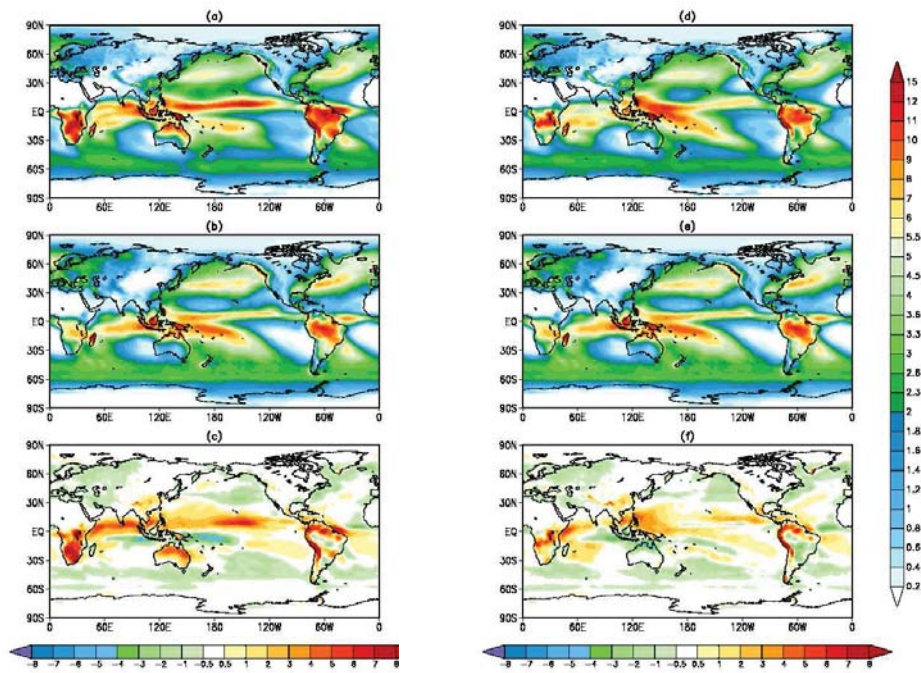me as a) but the difference, experiment 6 minus experiment 5, d) December-January-February specific humidity in $\mathrm{g\,kg^{-1}}$ from experiment 6 (MERRA AGCM-like), e) same as d) but from experiment 5, f) same as d) but the difference, experiment 6 minus experiment 5.

Fig. 12. December-January-February total precipitation in $\mathrm{mm\ day^{-1}}$ from a) experiment 6 (MERRA AGCM-like), b) GPCP, c) the difference, experiment 6 minus GPCP, d) experiment 5 (MERRA2 AGCM-like), e) GPCP, and f) the difference, experiment 5 minus GPCP.
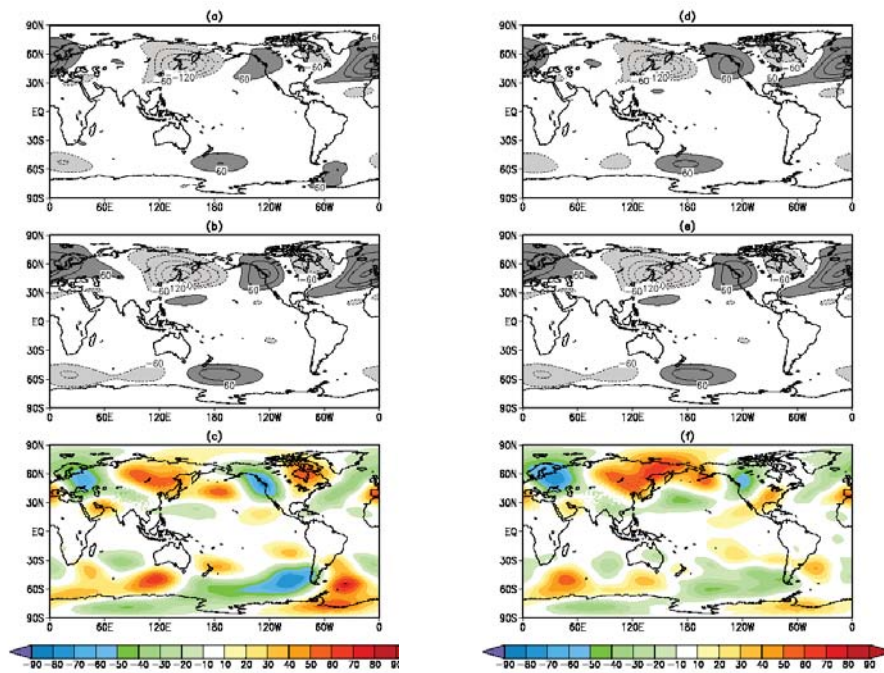
Fig. 13. December-January-February 300 mb Eddy Height Climatology in m from a) experiment 6 (MERRA AGCM-like), b) MERRA, c) the difference, experiment 6 minus MERRA, d) experiment 5 (MERRA2 AGCM-like), e) MERRA, and f) the difference, experiment 5 minus MERRA.
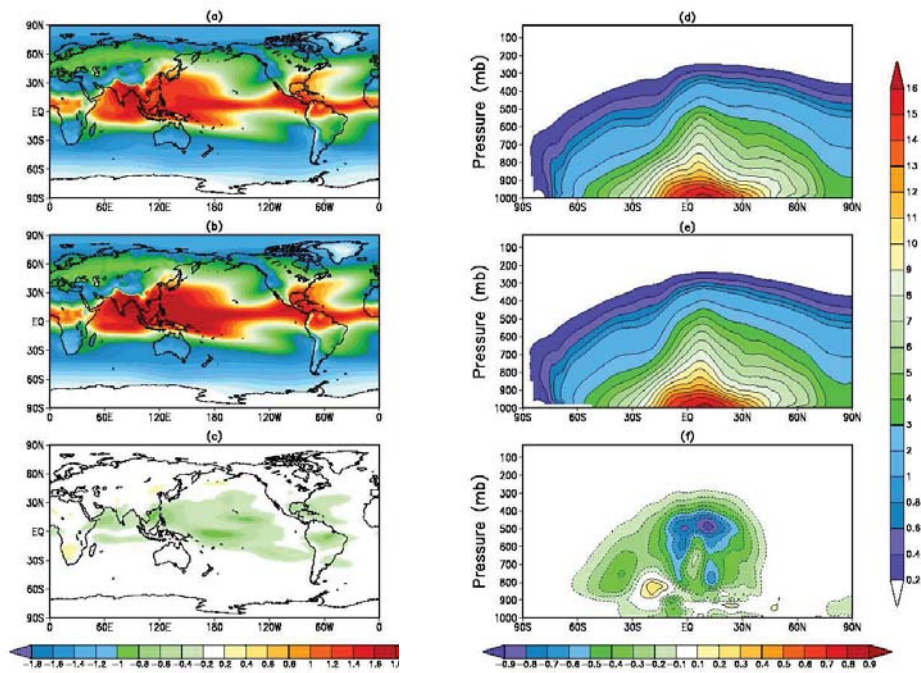
Fig. 14. a) June-July-August total precipitable water in mm from experiment 6 (MERRA AGCM-like), b) same as a) but from experiment 5, c) same as a) but the difference, experiment 6 minus experiment 5, d) June-July-August specific humidity in $g\,kg^{-1}$ from experiment 6 (MERRA AGCM-like), e) same as d) but from experiment 5, f) same as d) but the difference, experiment 6 minus experiment 5.
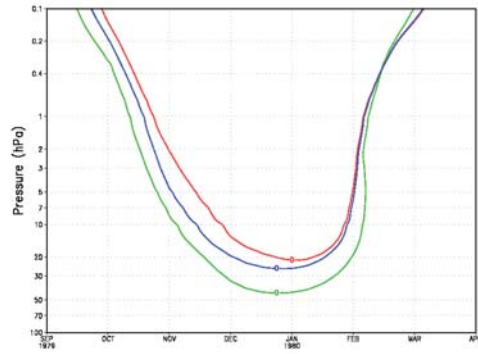
Fig. 15. 30-year averaged annual cycle of zonal mean zonal wind, averaged from 70S to 50S latitude in $m\ sec^{-2}$ from Experiment 7 in red (MERRA AGCM-like), experiment 6 in blue (MERRA2 AGCM-like) and MERRA in green
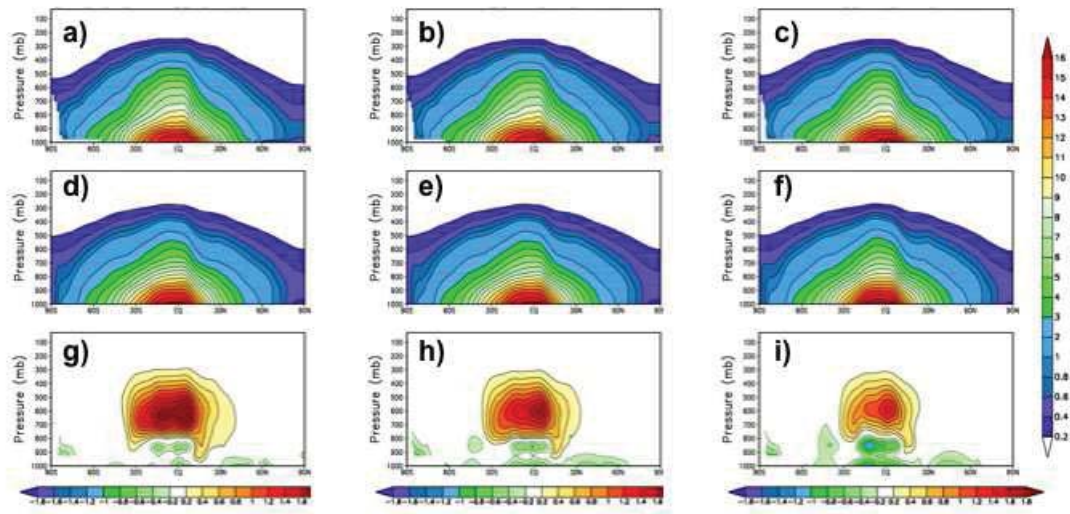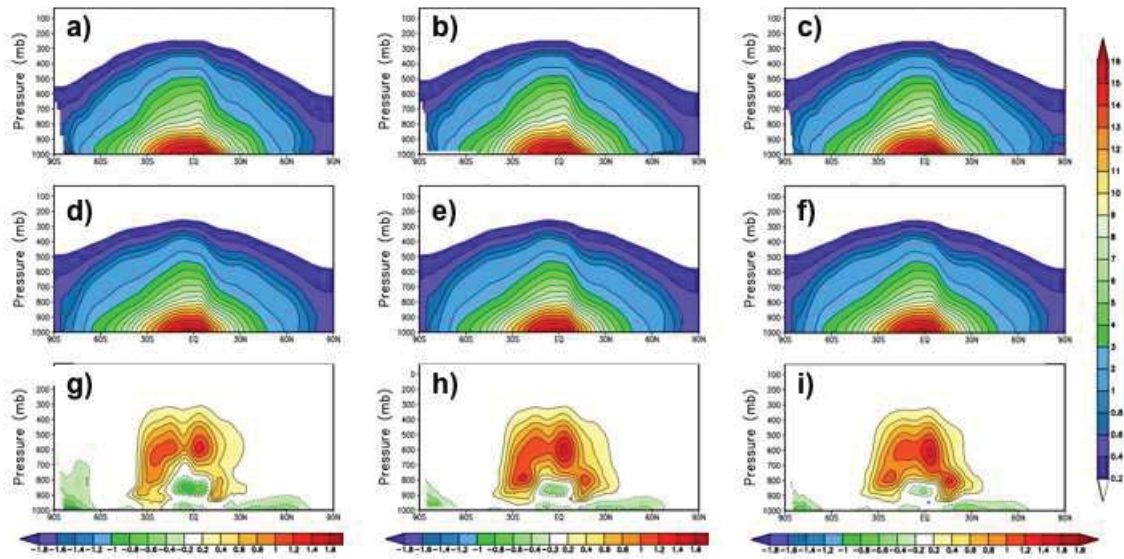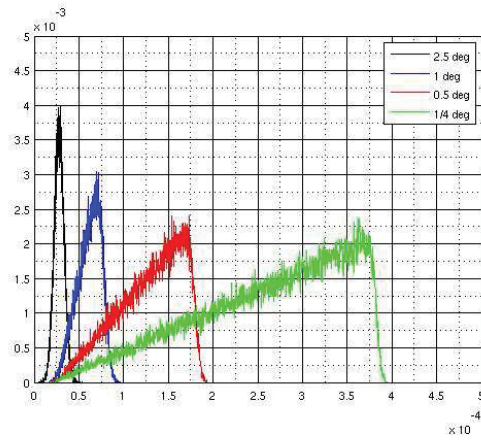
Fig. 16.

Fig. 17.

Fig. 18. The probability distribution function for the mimimum entrainment allowed by the cumulus parameterization for different AGCM horizontal resolutions. Black line is for 2 degree, blue for 1 degree, red for 1/2 degree and green for 1/4 degree.
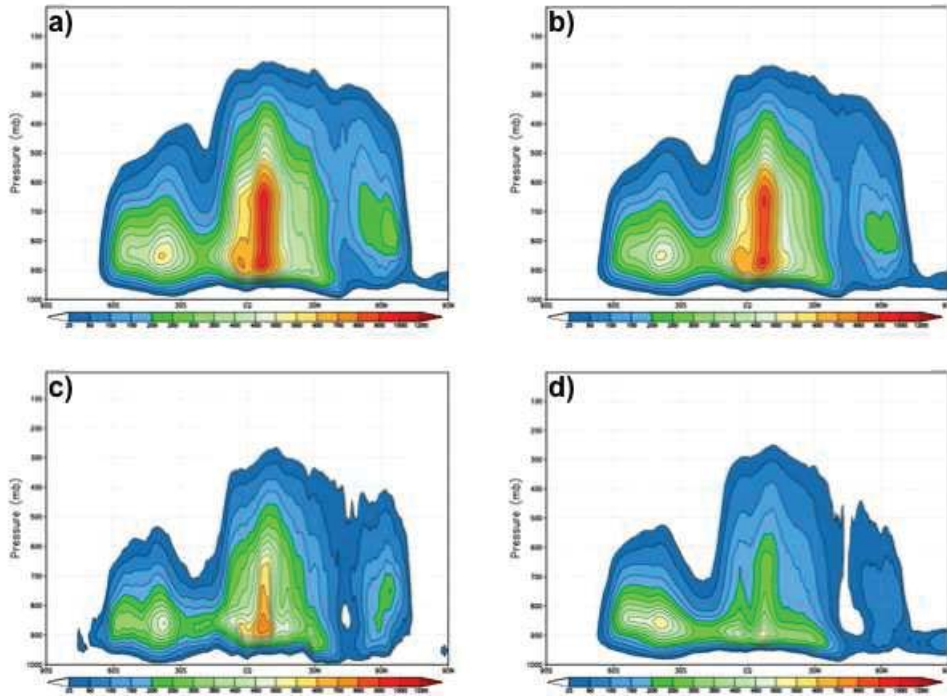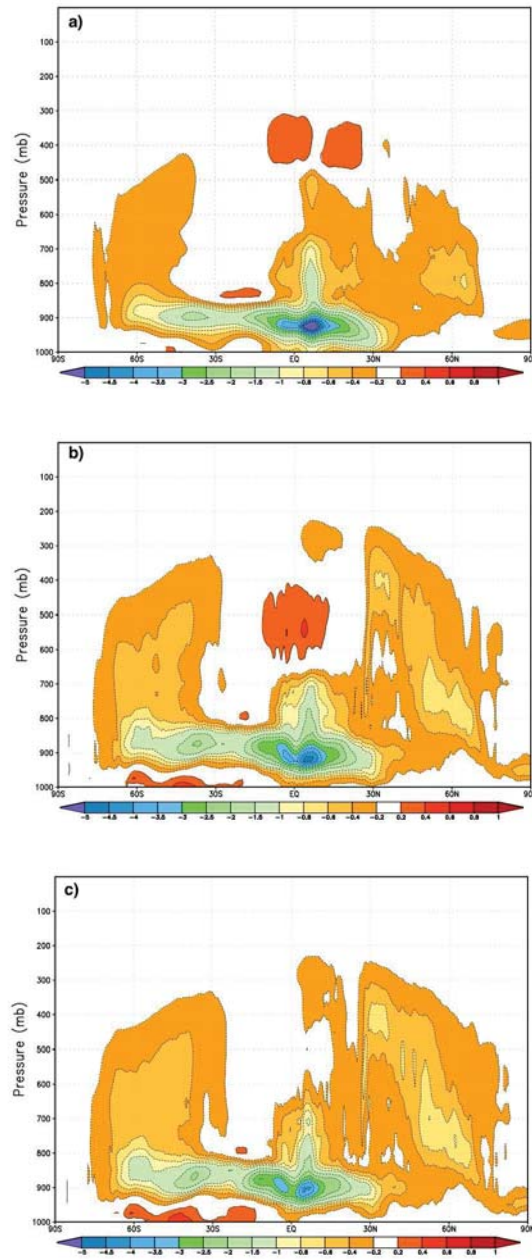
Fig. 19.

Fig. 20.

Table 1. Changes in GCM Algorithms from MERRA to Fortuna

Module	Algorithm Change	Comments
Moist	Increased re-evaporation of precipitation	Fundamental change in model climate
	Modified autoconversion	Fundamental change in model climate
	Modified effective radius of cloud drops	Fundamental change cloud forcing
	Anvil fractions cut in half	Fundamental change cloud forcing
	Autoconvert 'warm fog'	Important change in coupled simulations
	New critical RH with resolution dependance	Substantial change in simulated moisture
	Cloud base set at PBL depth	Remove clouds detraining below PBL height
	RAS time scale no longer depends on turbulence	
	Stochastic RAS with resolution dependance	Substantial impact at high resolution
Turb	Remove restrictions on diffusion from Louis	Increase near surface diffusion
	Reformulate turbulent length scale in Louis	
	Reduce Lock scheme when there is wind shear	Impact on marine PBL
	Reduce cloud top entrainment for Lock plumes	Impact on marine PBL
Surf	Implement Helfand and Schubert scheme	
	Remove viscous sublayer over land surfaces	Improve land temperatures
	Change ocean roughness for middle wind regimes	Reduce wind bias in S. Ocean
	Change ocean roughness high wind regimes	Increase tropical cyclone intensity
Land Surf	Changed parameters for evapotranspiration	Impact on ratio of surface to canopy evaporation
GW Drag	Changed profile of background drag	Substantial impact on QBO
	Added intermittency of drag	Impact on timing of winter jet breakup

Table 2. Experiments to attribute MERRA to Fortuna AGCM simulation changes to changes in parameterizations.

Experiment	Description
Control	
Exp 1	Back off change in ocean roughness
Exp 2	Exp 1 + Back off gravity wave background drag and surface hydrology
Exp 3	Exp 2 + use old surface layer parameterization
Exp 4	Exp 3 + Back off increase of Richardson-number diffusion
Exp 5	Exp 4 + Back off decrease of critical RH aloft and decrease below
Exp 6	Exp 5 + Back off increase of all re-evaporation
Exp 7	Exp 6 + Back off gravity wave drag intermittency